On pressure and velocity boundary conditions for the lattice Boltzmann BGK model

Qisu Zou
Theoretical Division, Los Alamos National Lab, Los Alamos, New Mexico 87545
and Department of Mathematics, Kansas State University, Manhattan, Kansas 66506

Xiaoyi He
Center for Nonlinear Studies and Theoretical Biology and Biophysics Group, Los Alamos National Laboratory, Los Alamos, New Mexico 87545

(Received 10 August 1995; accepted 24 February 1997)

Pressure (density) and velocity boundary conditions are studied for 2-D and 3-D lattice Boltzmann BGK models (LBGK) and a new method to specify these conditions is proposed. These conditions are constructed in consistency with the wall boundary condition, based on the idea of bounceback of the non-equilibrium distribution. When these conditions are used together with the incompressible LBGK model [J. Stat. Phys. **81**, 35 (1995)] the simulation results recover the analytical solution of the plane Poiseuille flow driven by a pressure (density) difference. The half-way wall bounceback boundary condition is also used with the pressure (density) inlet/outlet conditions proposed in this paper and in Phys. Fluids **8**, 2527 (1996) to study 2-D Poiseuille flow and 3-D square duct flow. The numerical results are approximately second-order accurate. The magnitude of the error of the half-way wall bounceback boundary condition is comparable with that of other published boundary conditions and it has better stability behavior. © *1997 American Institute of Physics.* [S1070-6631(97)03406-5]

I. INTRODUCTION

The lattice Boltzmann equation (LBE) method has achieved great success for simulation of transport phenomena in recent years. Among different LBE methods, the lattice Boltzmann BGK model is considered more robust.[1] For example, the 2-D triangular LBGK model with the boundary condition proposed in Ref. 2 generates results of machine accuracy for plane Poiseuille flow with external forcing to drive the flow. In practice, however, a flow is often driven by pressure difference, and the pressure gradient in many cases cannot be replaced by an external force in LBGK computations. In this situation, boundary conditions such as prescribed pressure or velocity on flow boundaries (e.g., inlet and outlet in a pipe flow) can be used to drive the flow.

In LBE methods, the specification of a pressure difference amounts to specification of a density difference. Early work[3] on pressure (density) flow boundary conditions assigned the equilibrium distribution, computed with the specified density and velocity, to the distribution function. This method introduces significant errors. Skordos[4] proposed to add the first-order approximation of the distribution, given by the Chapman–Enskog expansion, to the equilibrium distribution. The scheme requires the gradient of density and velocities, which can be approximated by a finite-difference formula. Inamuro *et al.*[5] and Maier *et al.*[6] proposed new boundary conditions for LBE simulations. In their simulation of Poiseuille flow with pressure (density) gradient, the pressure boundary condition was treated differently than their wall boundary condition. Chen *et al.*[7] also proposed a general way to specify boundary conditions, including flow boundary conditions. In this paper, we propose a way to specify pressure or velocity on flow boundaries, based on the idea of bounceback of the non-equilibrium distribution. When applied to the modified LBGK model, these boundary conditions produce results of machine accuracy for 2-D Poiseuille flow with pressure (density) or velocity inlet/outlet conditions.

All the proposed new boundary conditions (Refs. 2, 5, 6, 7) including the boundary conditions in this paper yield improved accuracy compared to the bounceback boundary condition. However, they are difficult to implement for general geometries, because there is a need to distinguish distribution functions according to their orientation to the wall, and, there are additional or different treatments at corner nodes. On the other hand, the complete bounceback scheme does not distinguish among distribution functions and is very easy to implement in a computer code, which is considered one of the advantages of the LGA or LBE methods. Moreover, the bounceback scheme with the wall located half-way between a flow node and a bounceback node (it will be called ''half-way wall bounceback'' thereafter) is shown theoretically to produce results of second-order accuracy for the simple flows considered.[8,9] In this paper, the half-way wall bounceback boundary condition and two flow boundary conditions are applied to the 2-D Poiseuille flow and a 3-D square duct flow using the d2q9i and d3q15i lattice Boltzmann models, respectively.

II. GOVERNING EQUATION

The square lattice LBGK model (d2q9) is expressed as (Refs. 10–12):

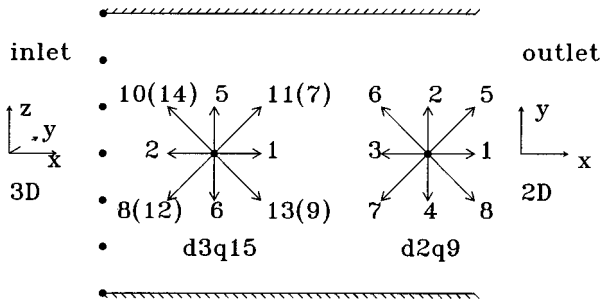

FIG. 1. Schematic plot of velocity directions of the 2-D (d2q9) model and projection of the 3-D (d3q15) model in a channel. In the 3-D model, The y-axis is pointing into the paper, so are velocity directions 3, 7, 9, 12, 14 (they are in parentheses if shown), while the velocity directions 4, 8, 10, 11, 13 are pointing out. Velocity directions 3, 4 have a projection at the center and are not shown in the figure.

$$f_i(\mathbf{x}+\delta\mathbf{e}_i,t+\delta)-f_i(\mathbf{x},t)=-\frac{1}{\tau}[f_i(\mathbf{x},t)-f_i^{(eq)}(\mathbf{x},t)],$$
$$i=0,1,\ldots,8, \tag{1}$$

where the equation is written in physical units. Both the time step and the lattice spacing have the value of δ in physical units. $f_i(\mathbf{x},t)$ is the density distribution function along the direction $\mathbf{e}_i$ at $(\mathbf{x},t)$. The particle speed $\mathbf{e}_i$'s are given by $\mathbf{e}_i=(\cos(\pi(i-1)/2),\sin(\pi(i-1)/2),i=1,2,3,4,$ and $\mathbf{e}_i=\sqrt{2}(\cos(\pi(i-4-\frac{1}{2})/2),\sin(\pi(i-4-\frac{1}{2})/2),i=5,6,7,8.$ Rest particles of type 0 with $\mathbf{e}_0=0$ are also allowed (see Fig. 1). The right hand side represents the collision term and τ is the single relaxation time which controls the rate of approach to equilibrium. The density per node, ρ, and the macroscopic flow velocity, $\mathbf{u}=(u_x,u_y)$, are defined in terms of the particle distribution function by

$$\sum_{i=0}^{8} f_i=\rho, \quad \sum_{i=1}^{8} f_i\mathbf{e}_i=\rho\mathbf{u}. \tag{2}$$

The equilibrium distribution functions $f_i^{(eq)}(\mathbf{x},t)$ depend only on local density and velocity and they can be chosen in the following form (the model d2q9[11]):

$$f_i^{(eq)}=t_i\rho\left[1+3(\mathbf{e}_i\cdot\mathbf{u})+\frac{9}{2}(\mathbf{e}_i\cdot\mathbf{u})^2-\frac{3}{2}\mathbf{u}\cdot\mathbf{u}\right],$$
$$t_0=\frac{4}{9}, \quad t_i=\frac{1}{9}, \quad i=1:4; \quad t_i=\frac{1}{36}, \quad i=5:8. \tag{3}$$

A Chapman–Enskog procedure can be applied to Eq. (1) to derive the macroscopic equations of the model. They are given by the continuity equation [with an error term $O(\delta^2)$ being omitted]

$$\frac{\partial\rho}{\partial t}+\nabla\cdot(\rho\mathbf{u})=0, \tag{4}$$

and the momentum equation [with terms of $O(\delta^2)$ and $O(\delta u^3)$ being omitted]

$$\partial_t(\rho u_\alpha)+\partial_\beta(\rho u_\alpha u_\beta)=-\partial_\alpha(c_s^2\rho)+\partial_\beta(2\nu\rho S_{\alpha\beta}), \tag{5}$$

where the Einstein summation convention is used. $S_{\alpha\beta}=\frac{1}{2}(\partial_\alpha u_\beta+\partial_\beta u_\alpha)$ is the strain-rate tensor. The pressure is given by $p=c_s^2\rho$, where c_s is the speed of sound with $c_s^2=\frac{1}{3}$, and $\nu=[(2\tau-1)/6]\delta$, with ν being the kinematic viscosity. The form of the error terms and the derivation of these equations can be found in Refs. 13 and 14.

For the 2-D case, we will take Poiseuille flow as an example to study the pressure (density) or velocity inlet/outlet condition. The analytical solution of Poiseuille flow in a channel of width $2L$ is given by

$$u_x=u_0\left(1-\frac{y^2}{L^2}\right), \quad u_y=0, \quad \frac{\partial p}{\partial x}=-G, \quad \frac{\partial p}{\partial y}=0, \tag{6}$$

where the pressure gradient G is a constant related to the centerline velocity u_0 by

$$G=2\rho\nu u_0/L^2, \tag{7}$$

and the flow density ρ is a constant. The Reynolds number is defined as $\mathrm{Re}=u_0(2L)/\nu$.

Poiseuille flow is an exact solution of the steady-state incompressible Navier–Stokes equations with constant density ρ_0:

$$\nabla\cdot\mathbf{u}=0, \tag{8}$$

$$\partial_\beta(u_\alpha u_\beta)=-\partial_\alpha\left(\frac{p}{\rho_0}\right)+\nu\partial_{\beta\beta}u_\alpha. \tag{9}$$

The steady-state macroscopic equations of the LBGK model are different from the incompressible Navier–Stokes equations, Eqs. (8) and (9), by terms containing the spatial derivative of ρ. These discrepancies are called compressibility error in the LBE model. Thus, when pressure (density) gradient drives the flow, u_x in a LBGK simulation increases in the x-direction, and the velocity profile is no longer parabolic. For a fixed Mach number (u_0 fixed), as $\delta\to0$, the velocity of the LBGK simulation will not converge to the velocity in Eq. (6) because the compressibility error becomes dominant. This makes the comparison of u_x with the analytical velocity of Poiseuille flow somehow ambiguous.

To make a more accurate study of Poiseuille flow with pressure (density) or velocity flow boundary conditions, we use the d2q9i incompressible LBGK model proposed in Ref. 15, with the following equilibrium distributions:

$$f_i^{(eq)}=t_i\left[\rho+3\mathbf{e}_i\cdot\mathbf{v}+\frac{9}{2}(\mathbf{e}_i\cdot\mathbf{v})^2-\frac{3}{2}\mathbf{v}\cdot\mathbf{v}\right], \quad t_0=\frac{4}{9},$$
$$t_i=\frac{1}{9}, \quad i=1:4; \quad t_i=\frac{1}{36}, \quad i=5:8 \tag{10}$$

and

$$\sum_{i=0}^{8} f_i=\sum_{i=0}^{8} f_i^{(eq)}=\rho, \quad \sum_{i=1}^{8} f_i\mathbf{e}_i=\sum_{i=1}^{8} f_i^{(eq)}\mathbf{e}_i=\mathbf{v}, \tag{11}$$

where $\mathbf{v}=(v_x,v_y)$ (like the momentum in the ordinary LBGK model) is used to represent the flow velocity. The macroscopic equations of d2q9i in the steady-state case (apart from error terms of $O(\delta^2)$)]

$$\nabla\cdot\mathbf{v}=0, \tag{12}$$

$$\partial_\beta(v_\alpha v_\beta) = -\partial_\alpha(c_s^2\rho) + \nu\partial_{\beta\beta}v_\alpha, \tag{13}$$

are exactly the steady-state incompressible Navier–Stokes equation with constant density ρ_0. In this model d2q9i, pressure is related to the calculated density by $c_s^2\rho = p/\rho_0$ ($c_s^2 = 1/3$), and $\nu = [(2\tau - 1)/6]\delta$. The quantity p/ρ_0 will be called the effective pressure. Although the macroscopic equations of d2q9i in the steady-state case have an error of $O(\delta^2)$ with respect to the steady-state Navier–Stokes equation, for some special flows like Poiseuille flow, this error disappears with suitable boundary conditions.

The 3-D 15-velocity LBGK model d3q15 is based on the LBGK equation, Eq. (1) with $i = 0,1,\ldots,14$, where $\mathbf{e}_i, i = 0,1,\ldots,14$ are the column vectors of the following matrix:

$$E = \begin{bmatrix} 0 & 1 & -1 & 0 & 0 & 0 & 0 & 1 & -1 & 1 & -1 & 1 & -1 & 1 & -1 \\ 0 & 0 & 0 & 1 & -1 & 0 & 0 & 1 & -1 & 1 & -1 & -1 & 1 & -1 & 1 \\ 0 & 0 & 0 & 0 & 0 & 1 & -1 & 1 & -1 & -1 & 1 & 1 & -1 & -1 & 1 \end{bmatrix},$$

and $\mathbf{e}_i, i = 1,\ldots,6$ are classified as type I, $\mathbf{e}_i, i = 7,\ldots,14$ are classified as type II. The density per node, ρ, and the macroscopic flow velocity, $\mathbf{u} = (u_x, u_y, u_z)$, are defined in terms of the particle distribution function by

$$\sum_{i=0}^{14} f_i = \rho, \quad \sum_{i=1}^{14} f_i\mathbf{e}_i = \rho\mathbf{u}. \tag{14}$$

The equilibrium can be chosen as

$$\begin{aligned} f_0^{(eq)} &= \frac{1}{8}\rho - \frac{1}{3}\rho\mathbf{u}\cdot\mathbf{u}, \\ f_i^{(eq)} &= \frac{1}{8}\rho + \frac{1}{3}\rho\mathbf{e}_i\cdot\mathbf{u} + \frac{1}{2}\rho(\mathbf{e}_i\cdot\mathbf{u})^2 - \frac{1}{6}\rho\mathbf{u}\cdot\mathbf{u}, \quad i \in I, \\ f_i^{(eq)} &= \frac{1}{64}\rho + \frac{1}{24}\rho\mathbf{e}_i\cdot\mathbf{u} + \frac{1}{16}\rho(\mathbf{e}_i\cdot\mathbf{u})^2 - \frac{1}{48}\rho\mathbf{u}\cdot\mathbf{u}, \\ & \quad i \in II. \end{aligned} \tag{15}$$

The macroscopic equations of the model is the same as Eqs. (4) and (5) with $c_s^2 = 3/8$, and $\nu = (2\tau - 1)\delta/6$. The incompressible model d3q15i is constructed from these formulas in a similar way as in d2q9i.

III. PRESSURE AND VELOCITY BOUNDARY CONDITIONS FOR THE LBGK MODEL

In this section a new boundary condition is proposed based on the idea of bounceback of the non-equilibrium part. As an example, take the case of a bottom node in Fig. 1. The boundary is aligned with the x-direction with f_4, f_7, f_8 pointing into the wall. After streaming, $f_0, f_1, f_3, f_4, f_7, f_8$ are known. Suppose that u_x, u_y are specified on the wall and we want to use Eq. (2) to determine f_2, f_5, f_6 and ρ (originated in Ref. 2), which can be put into the form

$$f_2 + f_5 + f_6 = \rho - (f_0 + f_1 + f_3 + f_4 + f_7 + f_8), \tag{16}$$

$$f_5 - f_6 = \rho u_x - (f_1 - f_3 - f_7 + f_8), \tag{17}$$

$$f_2 + f_5 + f_6 = \rho u_y + (f_4 + f_7 + f_8). \tag{18}$$

Consistency of Eqs. (16) and (18) gives

$$\rho = \frac{1}{1 - u_y}[f_0 + f_1 + f_3 + 2(f_4 + f_7 + f_8)]. \tag{19}$$

However, f_2, f_5 and f_6 remain undetermined. To close the system, we assume the bounceback rule is still correct for the *non-equilibrium part* of the particle distribution normal to the boundary (in this case, $f_2 - f_2^{(eq)} = f_4 - f_4^{(eq)}$). With f_2 known, f_5, f_6 can be found, thus

$$\begin{aligned} f_2 &= f_4 + \frac{2}{3}\rho u_y, \\ f_5 &= f_7 - \frac{1}{2}(f_1 - f_3) + \frac{1}{2}\rho u_x + \frac{1}{6}\rho u_y, \\ f_6 &= f_8 + \frac{1}{2}(f_1 - f_3) - \frac{1}{2}\rho u_x + \frac{1}{6}\rho u_y. \end{aligned} \tag{20}$$

The collision step is applied to the boundary nodes also. For non-slip boundaries, this boundary condition is reduced to that in Ref. 6. A detailed discussion of implementation of boundary conditions on stationary walls in the 3-D case was given in Ref. 6.

Now let us turn to the pressure (density) flow boundary condition. Suppose pressure (density) is to be specified on a flow boundary (take the inlet in Fig. 1 as an example) along the y-direction, and that u_y is also specified (e.g., $u_y = 0$ at the inlet in a channel flow). After streaming, f_2, f_3, f_4, f_6, f_7 are known, in addition to $\rho = \rho_{in}$, $u_y = 0$. We need to determine u_x and f_1, f_5, f_8 from Eq. (2) as follows:

$$f_1 + f_5 + f_8 = \rho_{in} - (f_0 + f_2 + f_3 + f_4 + f_6 + f_7), \tag{21}$$

$$f_1 + f_5 + f_8 = \rho_{in}u_x + (f_3 + f_6 + f_7), \tag{22}$$

$$f_5 - f_8 = -f_2 + f_4 - f_6 + f_7. \tag{23}$$

Consistency of Eqs. (21) and (22) gives

$$u_x = 1 - \frac{[f_0 + f_2 + f_4 + 2(f_3 + f_6 + f_7)]}{\rho_{in}}. \tag{24}$$

We use the bounceback rule for the non-equilibrium part of the particle distribution, normal to the inlet, to find $f_1 - f_1^{(eq)} = f_3 - f_3^{(eq)}$. With f_1 known, f_5, f_8 are obtained by the remaining two equations:

$$f_1 = f_3 + \frac{2}{3}\rho_{in} u_x,$$

$$f_5 = f_7 - \frac{1}{2}(f_2 - f_4) + \frac{1}{6}\rho_{in} u_x, \tag{25}$$

$$f_8 = f_6 + \frac{1}{2}(f_2 - f_4) + \frac{1}{6}\rho_{in} u_x.$$

The corner node at the inlet needs some special treatment. Take the bottom node at the inlet as an example. After streaming, f_3, f_4, f_7 are known, ρ is specified, and $u_x = u_y = 0$. We need to determine f_1, f_2, f_5, f_6, f_8. We use the bounceback rule for the non-equilibrium part of the particle distribution normal to the inlet and the boundary to find

$$f_1 = f_3 + (f_1^{(eq)} - f_3^{(eq)}) = f_3,$$
$$f_2 = f_4 + (f_2^{(eq)} - f_4^{(eq)}) = f_4. \tag{26}$$

Using f_1, f_2 in Eqs. (22), (23), we find

$$f_5 = f_7, \quad f_6 = f_8 = \frac{1}{2}[\rho_{in} - (f_0 + f_1 + f_2 + f_3 + f_4 + f_5 + f_7)]. \tag{27}$$

A similar procedure can be applied to the top inlet node and outlet nodes.

The specification of velocities u_x, u_y at a flow boundary (take the inlet in Fig. 1 as an example) is actually equivalent to a velocity wall boundary condition and can be handled in the same way as given at the beginning of the section. The effect of specifying velocity at the inlet is similar to specifying pressure (density) at the inlet, since both conditions will generate a density difference in the flow.

At the intersection of two perpendicular boundaries, such as the inlet bottom (non-slip boundary), special treatment is needed. After streaming, f_1, f_2, f_5, f_6, f_8 need to be determined. Using bounceback for the normal distributions gives

$$f_1 = f_3, \quad f_2 = f_4.$$

Expressions of x, y momenta give

$$f_5 - f_6 + f_8 = -(f_1 - f_3 - f_7) = f_7,$$
$$f_5 + f_6 - f_8 = -(f_2 - f_4 - f_7) = f_7, \tag{28}$$

or

$$f_5 = f_7,$$

$$f_6 = f_8 = \frac{1}{2}[\rho - (f_0 + f_1 + f_2 + f_3 + f_4 + f_5 + f_7)], \tag{29}$$

but there are no more equations available to determine ρ. In this situation, since ρ is expected to be constant at the inlet, ρ at the inlet bottom node can be taken as the ρ of its neighboring flow node, thus the velocity inlet condition is specified.

From the discussion given above, we can unify the derivation of boundary conditions which are aligned with the lattice directions in 2-D as the following

• Given u_x, u_y, find ρ and unknown f_i's.

• Given ρ and the velocity along the boundary, find the velocity normal to the boundary and unknown f_i's.

If a flow boundary is not aligned with lattice directions, schemes based on extrapolations like the ones in Refs. 7 and 6 could be developed.

The velocity wall boundary condition and flow boundary conditions for d2q9i are similar to that of d2q9 presented above. The derivation is based on equations $\Sigma_{i=0}^{8} f_i = \rho$ and $\Sigma_{i=1}^{8} \mathbf{e}_i f_i = \mathbf{v}$ and hence some modifications are needed. For the wall boundary condition, Eq. (19) is replaced by

$$\rho = v_y + [f_0 + f_1 + f_3 + 2(f_4 + f_7 + f_8)], \tag{30}$$

and in Eq. (20), $\rho u_x, \rho u_y$ are replaced by v_x, v_y, respectively. For the pressure flow boundary condition, Eq. (24) is replaced by

$$v_x = \rho_{in} - [f_0 + f_2 + f_4 + 2(f_3 + f_6 + f_7)], \tag{31}$$

and in Eq. (25), $\rho_{in} u_x$ is replaced by v_x.

The flow to be studied in the 3-D case is the square duct flow with the x-direction being the flow direction as shown in Fig. 1.

The pressure flow boundary condition for the model d3q15 is applied as follows. Take the case of an inlet node, as shown in Fig. 1, where the inlet is on the yz plane. After streaming, $f_i, (i = 0,2,3,4,5,6,8,10,12,14)$ are known. Suppose that $\rho_{in}, u_y = u_z = 0$ are specified on the inlet, and we need to determine $f_i, i = 1,7,9,11,13$ and u_x from Eq. (14). Similar to the derivation in d2q9, u_x is determined by a consistency condition as

$$\rho_{in} u_x = \rho_{in} - [f_0 + f_3 + f_4 + f_5 + f_6 + 2(f_2 + f_8 + f_{10} + f_{12} + f_{14})]. \tag{32}$$

The expression of x-momentum gives

$$f_1 + f_7 + f_9 + f_{11} + f_{13} = \rho_{in} u_x + (f_2 + f_8 + f_{10} + f_{12} + f_{14}). \tag{33}$$

If we use the bounceback rule for the non-equilibrium part of the particle distribution $f_i\,(i = 1,7,9,11,13)$ to set

$$f_i = f_{i+1} + (f_i^{(eq)} - f_{i+1}^{(eq)}), \tag{34}$$

then Eq. (33) is satisfied, and all f_i are defined. In order to get the correct y-,z-momenta, we further fix f_1 (the bounceback of non-equilibrium f_i in the normal direction) and modify f_7, f_9, f_{11}, f_{13} as in Ref. 6:

$$f_i \leftarrow f_i + \frac{1}{4} e_{iy} \delta_y + \frac{1}{4} e_{iz} \delta_z, \quad i = 7,9,11,13. \tag{35}$$

This modification leaves x-momentum unchanged but adds δ_y, δ_z to the y-,z-momenta, respectively. A suitable choice of δ_y and δ_z then gives the correct y-,z-momenta. Finally, we find

$$f_1 = f_2 + \frac{2}{3}\rho_{in} u_x,$$

$$f_i = f_{i+1} + \frac{1}{12}\rho_{in} u_x - \frac{1}{4}[e_{iy}(f_3 - f_4) + e_{iz}(f_5 - f_6)], \tag{36}$$

$$i = 7,9,11,13.$$

There is no special treatment at the wall of the inlet/outlet if bounceback is used there. Modification of the flow boundary condition for d3q15i is similar to d2q9i. The velocity flow boundary condition can be derived similarly.

IV. WALL BOUNDARY CONDITIONS FOR THE LBGK MODEL

The ''complete'' bounceback scheme which assigns each f_i the value of the f_j of its opposite direction with no relaxation on the bounceback nodes is very easy and convenient to apply. The treatment is independent of the direction of f_i's, which is one of the major advantages of the LGA and LBE methods. However, the bounceback rule with the wall placed at the bounceback nodes gives a first-order error in velocity. This has been shown analytically[9] for some simple flows and computationally[14] for 2-D cavity flows. Several theoretical studies have shown that if the wall is placed half-way between the bounceback row and the first flow row (''half-way wall bounceback''), the scheme gives a second-order accuracy[8,9,16,17] for some simple flows, including an inclined channel flow and a plane stagnation flow. For example, if the d2q9 model with half-way wall bounceback is used to simulate the 2-D Poiseuille flow with forcing, the error in velocity (it is the same for any node) is given by[9]

$$u_j^t - u_j = -\frac{u_0[4\tau(4\tau-5)+3]}{3}\delta^2, \tag{37}$$

where u_j^t, u_j are the analytical and computed x-velocity, respectively, and u_0 is the center velocity. For a fixed τ, the error is second-order in the lattice spacing δ. Of course, large value of τ will give large errors,[2,5] because the Chapman–Enskog procedure breaks down when τ is large. However, for τ between 0.5 and 1.25, the magnitude of the error given in (37) is less than or equal to $1.1\, u_0\delta^2$. Thus, it is worthwhile to consider this boundary condition in more general situations, especially in 3-D flows.

V. NUMERICAL RESULTS

In this section, we present numerical results using the models d2q9i and d3q15i. For 2-D Poiseuille flow, the width of the channel is assumed to be $2L=2$, and we use nx, ny lattice nodes on the x- and y-directions, thus, $\delta = 2/(ny-1)$. The initial condition is the equilibrium distribution, using a constant density ρ_0, and zero velocity. The steady-state is reached if

$$\frac{\Sigma_i\Sigma_j|v_x(i,j,t+\delta)-v_x(i,j,t)|+|v_y(i,j,t+\delta)-v_y(i,j,t)|}{\Sigma_i\Sigma_j|v_x(i,j,t)|+|v_y(i,j,t)|} \leqslant \delta\cdot Tol, \tag{38}$$

where Tol is a tolerance set to 10^{-12}. We also define the maximum relative error in velocity (v_x, v_y) as in Ref. 18:

$$err_m \equiv \max\frac{\sqrt{(u_x^t-v_x)^2+(u_y^t-v_y)^2}}{u_0}, \tag{39}$$

where u_x^t, u_y^t is the analytical velocity u_0 is the peak velocity, and the maximum is over the entire lattice.

We first present results using the pressure and velocity conditions given in this paper at all boundaries, including walls. The range of Re is from 0.0001 to 30.0; the range of τ is from 0.56 to 20.0 and the range of u_0 is from 0.001 to 0.4; the largest density difference simulated (not the limit) is $\rho_{in}=5.6$, $\rho_{out}=4.4$ with $nx=5, ny=3$ corresponding to an effective pressure gradient of $G'=0.1$, where G' is defined as $G'=-(1/\rho_0)(dp/dx)$. The magnitude of average density ρ_0 is 5, but it is irrelevant for the simulation.[15] All simulations in this paper use double-precision.

For all cases where the simulation is stable, the steady-state velocity, v_x, is uniform in the x-direction, and is accurate up to machine accuracy compared to the analytical solution in Eq. (6). The maximum of $|v_y|$ is on the order of 10^{-13}. For example, for $nx=5, ny=3, u_0=0.1, \tau=0.56$, Re $=10$, the maximum relative error in v_x is 0.1816×10^{-11}, while the maximum relative error in ρ is 0.3553×10^{-15}, and the maximum magnitude of v_y is 0.5551×10^{-15}. The results for other cases are similar to this example. In all simulations, the density is uniform in the cross channel direction, and linear in the flow direction. The computed and the analytical density gradients differ only at the 14th digit. It is also noticed that when a pressure (density) gradient drives Poiseuille flow, the maximum Reynolds number which makes the simulation stable is less than that with external forcing.

Similar results are obtained by specifying the analytical velocity profile given in Eq. (6) at the inlet and pressure (density) at the outlet, using the flow boundary conditions in this paper. In this case, there is a uniform pressure (density) difference in the region, which depends on u_0 and the outlet density.

We next present results for Poiseuille flow using pressure or velocity boundary conditions only at the flow boundaries, and using simple bounceback at the walls. For half-way wall bounceback, if there are ny nodes on the y-direction, then the first and last nodes are the bounceback nodes with the wall being located half-way between the bounceback node and the first flow node. There are $ly=ny-2$ lattice steps across the channel and the lattice spacing is $\delta=2/(ny-2)=2/ly$. The length of the channel is set to twice as the width. At the inlet/outlet, bounceback is also used at the nodes on the bounceback rows, thus, there is no special treatment for the corner nodes. Three combinations of inlet/outlet (I/O) conditions and wall conditions were tested.

(1) The flow boundary condition given in this paper with half-way wall bounceback.
(2) The flow boundary condition proposed in Ref. 7 with half-way wall bounceback. (It assumes an additional layer of nodes beyond the boundary flow nodes and uses an extrapolation formula to derive the incoming f_i's of the additional layer before streaming.)
(3) The I/O and wall conditions used in Ref. 7.

To study convergence, we fix τ and the Reynolds number and vary the lattice spacing, δ, from 1/2 to 1/32. The peak velocity, u_0, is reduced along with δ, to keep compressibility error of the same size as discretization error. Three examples are reported in Table I using the pressure boundary

TABLE I. Maximum relative errors for 2-D Poiseuille flow with pressure specified at the inlet and outlet. The results of three boundary conditions Nos. 1, 2, 3 are given. In each box, the upper figure is the error, and the lower figure is the ratio of two consecutive errors. The last column shows the order of convergence using least-squares fitting. The symbol (-2) represents 10^{-2}.

	lx	8	16	32	64	128	order
	ly	4	8	16	32	64	
	u_0	0.8333(−1)	0.4167(−1)	0.2084(−1)	0.1042(−1)	0.5208(−2)	
	No. 1	0.6031(−1)	0.1500(−1)	0.3729(−2)	0.9297(−3)	0.2324(−3)	2.005
Re = 10		4.021	4.023	4.011	4.000		
τ=0.6	No. 2	0.5917(−1)	0.1479(−1)	0.3699(−2)	0.9265(−3)	0.2352(−3)	1.995
		4.001	3.998	3.992	3.939		
	No. 3			unstable			
	u_0	0.2500	0.1250	0.6250(−1)	0.3125(−1)	0.1563(−1)	
	No. 1	0.3276(−1)	0.8319(−2)	0.2054(−2)	0.5111(−3)	0.1276(−3)	2.003
Re = 10		3.938	4.050	4.019	4.005		
τ=0.8	No. 2	0.3250(−1)	0.8125(−2)	0.2032(−2)	0.5085(−3)	0.1283(−3)	1 .997
		4.000	3.999	3.996	3.963		
	No. 3	0.1000	0.2500(−1)	0.6250(−2)	0.1563(−2)	0.3920(−3)	1.999
		4.000	4.000	3.999	3.987		
	u_0	0.5000(−1)	0.2500(−1)	0.1250(−1)	0.6250(−2)	0.3125(−2)	
	No. 1	0.5550(−1)	0.1441(−1)	0.3617(−2)	0.9021(−3)	0.2249(−3)	1.989
Re = 1		4.011	4.010	3.984	3.851		
τ=1.1	No. 2	0.5750(−1)	0.1437(−1)	0.3594(−2)	0.8984(−3)	0.2246(−3)	2. 000
		4.001	3.998	4.000	4.000		
	No. 3	0.5000(−1)	0.1250(−1)	0.3125(−2)	0.7812(−3)	0.1953(−3)	2.000
		4.000	4.000	4.000	4.000		

condition. The ratio of two consecutive maximum relative errors is also shown. The order of convergence, from a least-squares fitting, is shown in the last column. For the cases of Nos. 1, 2 with the half-way wall bounceback, the maximum relative velocity errors are similar and the convergence rate is consistent with second-order accuracy. The magnitude of the errors is close to that obtained using No. 3. The quantity Tol in Eq. (38) is set to 10^{-8}.

To study stability, we compared the 3 cases with a simple equilibrium scheme, which is known to be stable. This scheme imposes the equilibrium distribution at the flow boundaries. In the simulation of Poiseuille flow with bounceback at the walls, using the equilibrium scheme to prescribe velocity inlet and density outlet conditions, and with $lx=16, ly=8$, $u_0=0.1$. We obtained a maximum of Re 500. Once any boundary condition or flow boundary condition in any of the schemes in[2,5–7,18] or in this paper is used, the maximum Re number is reduced dramatically. For example, the maximum Re reduces to 63 and 56, respectively, for cases No. 1 and No. 2. The maximum Re further reduces to 12 for case No. 3. It is also noted that when the parameters are close to the region of instability, the simulation may have unusual large errors.

Simulations of 3-D square duct flow were performed using d3q15i and d3q15 with the pressure flow boundary condition. Only the results for d3q15i are reported, since the results of d3q15 are similar. The analytical solution of a flow in an infinitely long rectangular duct $-a\leqslant y\leqslant a, -b\leqslant z\leqslant b$, with x being the flow direction is given by[19]

$$u_x(y,z)=\frac{16a^2}{\mu\pi^3}\left(-\frac{dp}{dx}\right)\sum_{i=1,3,5,\ldots}^{\infty}(-1)^{(i-1)/2}\times\left[1-\frac{\cosh(i\pi z/2a)}{\cosh(i\pi b/2a)}\right]\frac{\cos(i\pi y/2a)}{i^3}. \tag{40}$$

We use $a=b=2$ in the simulations. Results of the following boundary conditions are reported.

(1) The flow boundary condition given in this paper with the half-way wall bounceback.
(2) The flow boundary condition in Ref. 7 with the half-way wall bounceback.
(3) The flow and wall boundary conditions in Ref. 7.
(4) The flow and wall boundary conditions in Ref. 6.
(5) The flow boundary condition in Ref. 7 with bounceback at wall nodes *without collision.*

Again, we fix τ and the Reynolds number, vary δ from 1/2 to 1/16, to study convergence. Three examples are reported in Table II. The quantity Tol in the 3-D version of Eq. (38) is set as 10^{-8}. From Table II, we can see that Nos. 1–4 all give an accuracy close to second order, and that the errors with half-way wall bounceback are comparable to those obtained using the boundary conditions in Refs. 7 and 6. On the other hand, bounceback without collision (No. 5) introduces an error of first-order throughout the flow. Thus, half-way wall bounceback has different behavior than bounceback without collision.

It is noted that the order of convergence for 3-D duct flow, with all boundary conditions, is lower than that for 2-D Poiseuille flows. For example, the ratios of errors at the highest resolution are not very close to 4 in some cases. It ap-

TABLE II. Maximum relative errors for 3-D square duct flow with pressure specified at the inlet and outlet. The results of five boundary conditions (Nos. 1–5) are given. In each box, the upper figure is the error, and the lower figure is the ratio of two consecutive errors. The last column shows the order of convergence using least-squares fitting.

	lx	8	16	32	64	order
	ly,lz	4	8	16	32	
	u_0	0.8333(−1)	0.4167(−1)	0.2083(−1)	0.1042(−1)	
	No. 1	0.4028	0.1054	0.2742(−1)	0.7289(−2)	1.931
Re = 10		3.822	3.844	3.762		
τ=0.6	No. 2		unstable			
	No. 3		unstable			
	No. 4	0.2210	0.5565(−1)	0.1293(−1)	0.3132(−2)	2.053
		3.971	4.304	4.128		
	u_0	0.1250	0.6250(−1)	0.3125(−1)	0.1563(−1)	
	No. 1	0.1382	0.3980(−1)	0.9805(−2)	0.2388(−2)	1.959
Re = 5		3.472	4.059	4.106		
τ=0.8	No. 2	0.1371	0.3659(−1)	0.9243(−2)	0.2310(−2)	1.966
		3.747	3.959	4.001		
	No. 3	0.3397	0.9563(−1)	0.2117(−1)	0.5741(−2)	1.984
		3.552	4.517	3.688		
	No. 4	0.8567(−1)	0.1543(−1)	0.4502(−1)	0.1278(−2)	1.998
		5.552	3.427	3.523		
	No. 5	0.6539	0.3345	0.1536	0.7935(−1)	1.025
		1.955	2.178	1.936		
	u_0	0.1000(−1)	0.5000(−2)	0.2500(−2)	0.1250(−2)	
	No. 1	0.2091	0.6537(−1)	0.1817(−1)	0.4807(−2)	1.818
Re = 0.2		3.199	3.598	3.780		
τ=1.1	No. 2	0.2114	0.6448(−1)	0.1787(−1)	0.4737(−2)	1.829
		3.279	3.608	3.772		
	No. 3	0.3109	0.7740(−1)	0.1966(−1)	0.4904(−2)	1.994
		4.017	3.937	4.009		
	No. 4	0.2070	0.4973(−1)	0.1277(−1)	0.3341(−2)	1.982
		4.162	3.894	3.822		

pears that in 3-D duct flow, the four edges pose additional difficulties to resolving the flow. Even with forcing, the density is not uniform in a cross section for the half-way wall bounceback or for boundary conditions in Refs. 7 and 6. Nevertheless, the order of convergence for 3-D duct flow is still close to 2. The half-way wall bounceback has a weaker convergence when $\tau>1$ while the boundary condition in Ref. 7 performs better as $\tau>1$ but worse as $\tau<1$.

We would like to point out that a second-order accuracy of the half-way wall bounceback in the flows considered does not imply a second-order accuracy for any flows. The statement can be applied to other boundary conditions as well. One is encouraged to do some tests on a simplified flow of the type of flows to be simulated.

VI. DISCUSSIONS

In this paper we have derived boundary conditions for the incompressible LBGK models, d2q9i and d3q15i, using a new way to specify flow boundary conditions based on bounceback of the non-equilibrium distribution. For the test problem of Poiseuille flow with pressure or velocity inlet/outlet conditions, the new method recovers the analytic solution within machine accuracy, and it is approximately of second-order accuracy for the 3-D channel flows with τ ranging from 0.6 to 1.2 in the simulations. The magnitude of the error is comparable with that using some published boundary conditions.

We have also observed that the half-way wall bounceback method is approximately second-order accurate for the channel flows considered, and conclude that it deserves serious consideration in a LBGK simulation.

ACKNOWLEDGMENTS

Discussions with R. Maier and R. Bernard are appreciated. Q. Z. would like to thank the Associated Western Universities, Inc. for providing a fellowship and to thank G. Doolen and S. Chen for helping to arrange his visit to the Los Alamos National Lab. Some computations are performed on the Convex Exempler SPP-1000 of Kansas State University. Q. Z. would like to thank National Science Foundation Grant No. DMR-9413513 which provided funds for the acquisition of the machine.

[1] S. Succi, D. d'Humières, Y. Qian, and S. A. Orszag, ''On the small-scale dynamical behavior of lattice BGK and lattice Boltzmann schemes,'' J. Sci. Comput. **8**, 219 (1993).

[2] D. R. Noble, S. Chen, J. G. Georgiadis, and R. O. Buckius, ''A consistent hydrodynamic boundary condition for the lattice Boltzmann method,'' Phys. Fluids **7**, 203 (1995).

[3]D. W. Grunau, ''Lattice methods for modeling hydrodynamics,'' Ph.D. thesis, Colorado State University, 1993.
[4]P. A. Skordos, ''Initial and boundary conditions for the lattice Boltzmann method,'' Phys. Rev. E **48**, 4823 (1993).
[5]T. Inamuro, M. Yoshino, and F. Ogino, ''A non-slip boundary condition for lattice Boltzmann simulations,'' Phys. Fluids **7**, 2928 (1996).
[6]R. S. Maier, R. S. Bernard, and D. W. Grunau, ''Boundary conditions for the lattice Boltzmann method,'' Phys. Fluids **8**, 1788 (1996).
[7]S. Chen, D. O. Martinez, and R. Mei, ''On boundary conditions in lattice Boltzmann methods,'' Phys. Fluids **8**, 2527 (1996).
[8]Q. Zou, S. Hou, and G. D. Doolen, ''Analytical solutions of the lattice Boltzmann BGK model,'' J. Stat. Phys. **81**, 319 (1995).
[9]X. He, Q. Zou, L. S. Luo, and M. Dembo, ''Analytic solutions of simple flows and non-slip boundary condition for the lattice Boltzmann BGK model,'' J. Stat. Phys. **87**, 115 (1997).
[10]S. Chen, H. Chen, D. O. Martinez, and W. H. Matthaeus, ''Lattice Boltzmann model for simulation of magnetohydrodynamics,'' Phys. Rev. Lett. **67**, 3776 (1991).
[11]Y. Qian, D. d'Humières, and P. Lallemand, ''Recovery of Navier–Stokes equations using a lattice-gas Boltzmann method,'' Europhys. Lett. **17**, 479 (1992).
[12]H. Chen, S, Chen, and W. H. Matthaeus, ''Recovery of Navier–Stokes equations using a lattice-gas Boltzmann method,'' Phys. Rev. A **45**, 5771 (1992).
[13]Y. H. Qian and S. A. Orszag, ''Lattice BGK models for Navier–Stokes equation,'' Europhys. Lett. **21**, 255 (1993).
[14]S. Hou, Q. Zou, S. Chen, G. D. Doolen, and A. C. Cogley, ''Simulation of cavity flow by the lattice Boltzmann method,'' J. Comput. Phys. **118**, 329 (1995).
[15]Q. Zou, S. Hou, S. Chen, and G. D. Doolen, ''An improved incompressible lattice Boltzmann model for time-independent flows,'' J. Stat. Phys. **81**, 35 (1995).
[16]R. Cornubert, D. d'Humières, and D. Levermore, ''A Knudsen layer theory for lattice gases,'' Physica D **47**, 241 (1991).
[17]I. Ginzbourg and P. M. Adler, ''Boundary flow condition analysis for the three-dimensional lattice Boltzmann model,'' J. Phys. II France **4**, 191 (1994).
[18]D. R. Noble, J. G. Georgiadis, and R.O. Buckius, ''Direct assessment of lattice Boltzmann hydrodynamics and boundary conditions for recirculating flows,'' J. Stat. Phys. **81**, 17 (1995).
[19]F. M. White, *Viscous Fluid Flow* (McGraw-Hill, New York, 1974), p. 123.